

Redefining the Shortest Path Problem Formulation of the Linear Non-Gaussian Acyclic Model: Pairwise Likelihood Ratios, Prior Knowledge, and Path Enumeration

HANS JARETT J. ONG, Nara Institute of Science and Technology, Japan

BRIAN GODWIN S. LIM, Nara Institute of Science and Technology, Japan

Effective causal discovery is essential for learning the causal graph from observational data. The linear non-Gaussian acyclic model (LiNGAM), a causal discovery technique, operates under the assumption of a linear data generating process with non-Gaussian noise in determining the causal graph. Its assumption of unmeasured confounders being absent, however, poses practical limitations. In response, empirical research has shown that the reformulation of LiNGAM as a shortest path problem (LiNGAM-SPP) addresses this limitation. Within LiNGAM-SPP, mutual information is chosen to serve as the measure of independence. A challenge is introduced – parameter tuning is now needed due to its reliance on k -nearest neighbors (k NN) mutual information estimators. The paper proposes a threefold enhancement to the LiNGAM-SPP framework.

First, the need for parameter tuning is eliminated by using the pairwise likelihood ratio in lieu of k NN-based mutual information. This substitution is validated on a general data generating process and benchmark real-world data sets, outperforming existing methods especially when given a larger set of features. The incorporation of prior knowledge is then enabled by a node-skipping strategy implemented on the graph representation of all causal orderings to eliminate violations based on the provided input of relative orderings. Flexibility relative to existing approaches is achieved. Last among the three enhancements is the utilization of the distribution of paths in the graph representation of all causal orderings. From this, crucial properties of the true causal graph such as the presence of unmeasured confounders and sparsity may be inferred. To some extent, the expected performance of the causal discovery algorithm may be predicted. The aforementioned refinements advance the practicality and performance of LiNGAM-SPP, showcasing the potential of graph-search-based methodologies in advancing causal discovery.

CCS Concepts: • **Computing methodologies** → **Causal reasoning and diagnostics**; • **Mathematics of computing** → **Causal networks**; • **Information systems** → *Data mining*.

Additional Key Words and Phrases: Causal discovery, shortest path problem, linear non-Gaussian acyclic model, unmeasured confounders.

ACM Reference Format:

Hans Jarett J. Ong and Brian Godwin S. Lim. yyyy. Redefining the Shortest Path Problem Formulation of the Linear Non-Gaussian Acyclic Model: Pairwise Likelihood Ratios, Prior Knowledge, and Path Enumeration. *ACM Trans. Knowl. Discov. Data.* vv, n, Article aaa (January yyyy), 18 pages. <https://doi.org/XXXXXXXX.XXXXXXX>

1 INTRODUCTION

Machine learning has achieved significant success by its ability to identify patterns in large sets of independent and identically distributed data. However, many of these techniques face difficulty with

Authors' addresses: Hans Jarett J. Ong, ong.hans_jarett.015@naist.ac.jp, Nara Institute of Science and Technology, Nara, Japan, 630-0192; Brian Godwin S. Lim, lim.brian_godwin_sy.la6@is.naist.jp, Nara Institute of Science and Technology, Nara, Japan, 630-0192.

Permission to make digital or hard copies of all or part of this work for personal or classroom use is granted without fee provided that copies are not made or distributed for profit or commercial advantage and that copies bear this notice and the full citation on the first page. Copyrights for components of this work owned by others than the author(s) must be honored. Abstracting with credit is permitted. To copy otherwise, or republish, to post on servers or to redistribute to lists, requires prior specific permission and/or a fee. Request permissions from permissions@acm.org.

© yyyy Copyright held by the owner/author(s). Publication rights licensed to ACM.

ACM 1556-4681/yyyy/01-ARTaaa

<https://doi.org/XXXXXXXX.XXXXXXX>

out-of-distribution generalization because they tend to disregard important information such as interventions in the world, domain shifts, and temporal structure [28]. Causal models, particularly graphical causal models [21, 22, 25], offer a solution to this problem by modeling the data generating process itself using causal graphs. This enables causal models to generalize out of distribution and to make interventional and counterfactual predictions. Aside from graphical causality, another well-established framework for causal inference is the potential outcomes framework [26, 38]. This paper, nonetheless, focuses solely on graphical causality.

While there are methods for estimating interventions and counterfactuals such as Pearl’s do-calculus and structural causal models (SCMs) [21–23], these require knowing the causal graph which is often unknown in practice. A straightforward approach to obtaining the causal graph is to construct it from domain knowledge. This process is often tedious and time-consuming, especially in settings with many features. Causal discovery methods resolve this by attempting to learn the causal structure from data. One such causal discovery method is the Linear Non-Gaussian Acyclic Model (LiNGAM) [29–31], which assumes a linear data generating process and noise terms with non-Gaussian distributions.

LiNGAM also assumes the absence of unmeasured confounders [30], which can be a significant limitation in practice. Several improvements to LiNGAM have been proposed in order to address this issue, one of which is the formulation of LiNGAM as a shortest path problem (LiNGAM-SPP) [34, 35]. LiNGAM-SPP identifies the causal ordering of the features by selecting the path that minimizes the mutual information of the noise terms. Although LiNGAM-SPP presents a promising solution to the challenge of unmeasured confounders, a notable drawback is its reliance on parameter tuning. This proves impractical in real-world scenarios where access to the underlying data generating process is unavailable.

In light of this, we introduce an enhanced version of LiNGAM-SPP that eliminates the need for parameter tuning and at the same time demonstrates superior performance and computational efficiency. In addition to its primary objective of addressing unmeasured confounders, the LiNGAM-SPP offers a unique perspective on the causal ordering problem. It allows us to view this problem as a path search problem, where each path corresponds to a potential causal ordering. This paper also explores other ways to leverage this path formulation beyond its initial purpose.

While the original LiNGAM-SPP papers [34, 35] have established that each possible path corresponds to a causal ordering and that the shortest path corresponds to the most likely true causal ordering, we ask: “Can we exploit other features of this path search space?” The answer is affirmative. We show that constrained searches where certain nodes are excluded correspond to incorporating prior knowledge and that this method of integrating knowledge is more flexible than those employed by LiNGAM [30] as it only imposes relative orderings.

Furthermore, we delve into another property of the path search space – the distribution of the measure of independence from all possible causal orderings. We demonstrate that this distribution can be used to infer key graph properties such as the presence of unmeasured confounders, graph sparsity, and even the potential performance of causal discovery algorithms.

In summary, our contribution is threefold.

- (1) **Improving LiNGAM-SPP:** We modify LiNGAM-SPP to eliminate the need for parameter tuning while yielding enhanced performance and computational efficiency.
- (2) **Incorporating Known Relative Ordering:** We expand LiNGAM-SPP to incorporate prior knowledge, requiring only relative ordering for better adaptability.
- (3) **Predicting Causal Graph Properties:** We develop predictive models using features derived from the path distributions of LiNGAM-SPP, specifically for predicting presence of unmeasured confounders, graph sparsity, and causal discovery algorithm performance.

2 PRELIMINARIES

In this section, we begin by briefly introducing graphical causality to provide context to the problem. Next, we review LiNGAM. Finally, we discuss LiNGAM-SPP and how it generalizes LiNGAM by framing it as a shortest path problem.

2.1 Graphical Causality

Graphical causality [21, 22, 25] uses directed acyclic graphs (DAGs) to represent causal relationships between variables. A DAG \mathcal{G} can represent a joint probability distribution P_X either as a factorized probability distribution or as an SCM.

The joint probability distribution P_X can be represented by a factorized probability distribution according to the Markov factorization property [25]. Using \mathcal{G} ,

$$P(X_1, \dots, X_n) = \prod_{i=1}^n P(X_i | \text{PA}_i^{\mathcal{G}}), \quad (1)$$

where each variable X_i corresponds to a node i in \mathcal{G} and $\text{PA}_i^{\mathcal{G}}$ denotes the variables corresponding to the parents of node i . When the edges of \mathcal{G} are causal, it is referred to as a causal graph.

SCMs, on the other hand, represent P_X in a slightly different way. In SCMs, each node i corresponds to a variable X_i , a deterministic function f_i , an exogenous variable or noise term U_i which are assumed to be jointly independent, and the probability distribution of U_i which capture the stochasticity of P_X [22, 28]. This is given by

$$X_i := f_i(\text{PA}_i, U_i). \quad (2)$$

SCMs provide a more expressive representation than causal graphs by explicitly modeling the causal relationships using deterministic functions. In Pearl's Ladder of Causation [23], SCMs are placed at a higher level than causal graphs. While both can represent interventions, only SCMs can capture counterfactual reasoning. Regardless, both of these representations require knowing the structure of the underlying DAG \mathcal{G} , which can be obtained through causal discovery methods. One of such methods is LiNGAM, which is discussed in the following section.

2.2 LiNGAM

LiNGAM [29–31] assumes an SCM with linear functions, non-Gaussian noise terms, and no unmeasured confounders. Specifically, this is represented as linear equations in matrix form

$$\mathbf{x} = \mathbf{B}\mathbf{x} + \mathbf{e}, \quad (3)$$

where \mathbf{B} is a strictly lower triangular adjacency matrix and the elements of \mathbf{e} are continuous non-Gaussian distributions with zero mean and nonzero variance. The strictly lower triangular adjacency matrix implies that each variable is expressed as the linear combination of the variables that precede it plus the noise term. In effect, LiNGAM aims to discover the causal ordering of the variables. Once the causal ordering is obtained, it is possible to determine which connections are zero using sparse regression methods [29, 39].

The original LiNGAM paper [30] uses independent components analysis (ICA) to estimate Eq. (3), which is why it is often called ICA-LiNGAM in literature [7, 29, 31, 33]. A shortcoming of ICA-LiNGAM, however, is that it does not guarantee convergence to a correct solution in a finite number of steps. To address this, DirectLiNGAM [31] was proposed.

DirectLiNGAM provides a causal ordering in the same number of steps as the number of variables. In each step, DirectLiNGAM selects the variable that is the most independent – with the smallest mutual information – from the least squares residuals of the remaining unselected variables. Subsequently, DirectLiNGAM removes the effect of the selected variable by reassigning the remaining

variables with the residuals from the least squares. This process iterates until the causal order is obtained [31].

DirectLiNGAM allows for various measures of independence [31]. While the original implementation uses a kernel-based mutual information estimator [31], it also discusses alternative measures such as the Hilbert-Schmidt independence criterion (HSIC) [8], a k NN-based mutual information estimator [16], and single nonlinear correlation [10]. Moreover, a measure known as the pairwise likelihood ratio (PLR) is introduced, with its efficacy as an independence measure for DirectLiNGAM demonstrated [12]. Despite its computational simplicity, PLR performs at least as well and sometimes even better than ICA-LiNGAM and kernel-based DirectLiNGAM, especially in cases with a limited number of data points relative to the data dimension or when the data is noisy. The computational efficiency of PLR also renders it significantly faster than the kernel-based DirectLiNGAM [12]. As of writing, the official `lingam` package [13] defaults to using PLR in its implementation of DirectLiNGAM.

2.3 LiNGAM-SPP

LiNGAM-SPP was introduced as a generalization of DirectLiNGAM [34]. Unlike DirectLiNGAM, which determines variable ordering by selecting the most independent feature at each step, LiNGAM-SPP seeks the ordering that minimizes the total mutual information across all steps. The authors of LiNGAM-SPP made the assumption, supported through simulations, asserting that LiNGAM-SPP can accurately determine the causal order even in the presence of unmeasured confounders [34]. This characteristic makes LiNGAM-SPP a generalization of DirectLiNGAM, as the latter assumes the absence of unmeasured confounders.

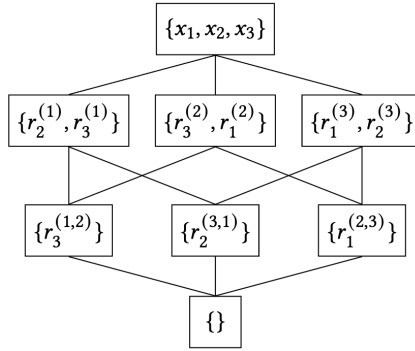


Fig. 1. LiNGAM-SPP: A shortest-path formulation of the causal ordering problem. Adapted from the LiNGAM-SPP paper [34] with slight changes in notation.

LiNGAM-SPP formulates the causal ordering problem as a graph search problem [34]. Figure 1 shows an example of how this is done for the three-variable case. In this graph, nodes represent candidate variables, edges represent some measure of independence, and the goal is to find a path from the starting node $\{x_1, x_2, x_3\}$ to the goal node $\{\}$. The selected variable and its independence can be inferred from the subscripts of candidate variables. For instance, the edge between $\{x_1, x_2, x_3\} \rightarrow \{r_2^{(1)}, r_3^{(1)}\}$ represents the mutual information if x_1 were selected as the first variable and its edge weight is the independence of x_1 vis-à-vis the residuals. Mathematically, this mutual information is denoted by $I(x_1, \{r_2^{(1)}, r_3^{(1)}\})$, where the residual is defined as

$$r_i^{(j)} = x_i - \frac{\text{cov}(x_i, x_j)}{\text{var}(x_j)} x_j. \quad (4)$$

Here, $r_i^{(j)}$ represents the residual when x_i is regressed on x_j . Similar to DirectLiNGAM, these residuals are stored for use in the next stage. For example, the edge $\{r_2^{(1)}, r_3^{(1)}\} \rightarrow \{r_3^{(1,2)}\}$ has an edge weight of $I(r_2^{(1)}, r_3^{(1,2)})$, the mutual information if x_2 were the second variable chosen after x_1 , where $r_3^{(1,2)}$ is the residual when $r_3^{(1)}$ is regressed on $r_2^{(1)}$.

The path formulation is made possible by the additive property of mutual information [16]. In notation,

$$I(X, Y, Z) = I(\{X, Y\}, Z) + I(X, Y). \quad (5)$$

This property facilitates the step-wise decomposition and calculation of mutual information to obtain the total mutual information. In the context of LiNGAM-SPP, we use this property to minimize $I(\epsilon_1, \epsilon_2, \dots, \epsilon_p)$, where ϵ_i represents the noise terms of the variables according to Eq. 3. We minimize this to satisfy the SCM property that the noise terms should be jointly independent [22, 28]. Referring to the example from Figure 1, if the causal order is x_1, x_2, x_3 , then the total mutual information is

$$I(\epsilon_1, \epsilon_2, \epsilon_3) = I(x_1, \{r_2^{(1)}, r_3^{(1)}\}) + I(r_2^{(1)}, r_3^{(1,2)}) + 0. \quad (6)$$

This is the sum of the edge weights along the path $\{x_1, x_2, x_3\} \rightarrow \{r_2^{(1)}, r_3^{(1)}\} \rightarrow \{r_3^{(1,2)}\} \rightarrow \{\}$, assuming all edges connecting to the $\{\}$ node have a value of 0, i.e., $I(r_i^{(j)}, \{\}) = 0$.

Finally, in order to look for the shortest path, LiNGAM-SPP uses Dijkstra's algorithm with lazy evaluation. The mutual information or the edge weights are only computed when needed. Please refer to either LiNGAM-SPP paper [34, 35] for a more detailed description of the algorithm.

3 METHODS

In this section, we present the implementation details of our contributions. We begin by discussing the enhancement of LiNGAM-SPP by using PLR as its mutual information estimator. Subsequently, we show how a constrained path search, which involves skipping certain nodes, can be used to incorporate prior knowledge of relative orderings. Finally, we discuss our approach for predicting causal graph properties from the path distribution.

3.1 Improving LiNGAM-SPP with PLR

The initial LiNGAM-SPP paper [34] demonstrated that using the k NN-based mutual information estimator [16] with LiNGAM-SPP led to superior performance compared to the HSIC-based DirectLiNGAM. However, a limitation was that the parameter k had to be tuned to achieve optimal performance. A subsequent study by the same authors [35] used copula entropy [18] as the mutual information estimator for LiNGAM-SPP, which, while achieving commendable performance, still relied on the k NN-based mutual information estimator [16]. In this study, we propose using the PLR as an alternative to the k NN-based mutual information estimator. Notably, PLR eliminates the need for parameter tuning, demonstrates superior performance, and is computationally more efficient.

PLR uses the likelihood ratio, or the difference between the log-likelihoods, to determine the causal direction between two non-Gaussian variables. For instance, in determining the causal direction between x and y , both standardized to have a mean of 0 and a variance of 1, PLR computes the difference between the log-likelihoods of both causal directions:

$$R = \frac{1}{T} \log L(x \rightarrow y) - \frac{1}{T} \log L(y \rightarrow x) \quad (7)$$

Here, the log-likelihoods are normalized by the sample size T . Given R , we can infer the correct direction: if R is positive, then $x \rightarrow y$; otherwise, $y \rightarrow x$. If $x \rightarrow y$, the SCM is $y = \rho x + d$, where $d \perp\!\!\!\perp x$. On the other hand, if $y \rightarrow x$, then the SCM is $x = \rho y + e$, where $e \perp\!\!\!\perp y$. Note

that the coefficient ρ is the same for both directions as it represents the correlation coefficient. Normally, computing R requires knowing the distributions of x, y, d, e . However, Hyvärinen (2013) [12] derived a practical approximation to compute this without prior knowledge of the distributions using differential entropy:

$$R \longrightarrow -H(x) - H(\hat{d}/\sigma_d) + H(y) + H(\hat{e}/\sigma_e) \quad (8)$$

Here, $\hat{d} = y - \rho x$ and $\hat{e} = x - \rho y$ represent the estimated residuals, and σ_d and σ_e denote their standard deviations. H represents the differential entropy, whose closed-form can be approximated using the approach by Hyvärinen (1998) [11]:

$$\hat{H}(u) = H(v) - k_1[E\{\log \cosh u\} - \gamma]^2 - k_2[E\{u \exp(-u^2/2)\}]^2 \quad (9)$$

where $H(v) = \frac{1}{2}(1 + \log 2\pi)$, and the constants have numerical values $k_1 \approx 79.047$, $k_2 \approx 7.4129$, and $\gamma \approx 0.37457$. This closed-form approximation contributes significantly to the efficiency of PLR.

In our implementation, we incorporated code from the `lingam` package [13], which currently defaults to using PLR in its DirectLiNGAM implementation. We adapted the relevant portions of this code to integrate the PLR measure into the LiNGAM-SPP framework with slight modifications. Specifically, the original implementation calculated the PLR independence measure m_i for each feature i as follows:

$$m_i = - \sum_j \min(0, [M]_{ij})^2 \quad (10)$$

where $[M]_{ij}$ is the PLR between feature i and j [12]. We introduce two modifications to adapt it to the shortest-path framework: First, we removed the negative sign and reformulated it as a minimization problem rather than a maximization one. Second, we normalized m_i by dividing it by the number of terms in the summation. This adjustment is crucial because failing to do so could result in earlier steps having larger values of m_i because they involve more terms. Such an imbalance in path measurements might pose challenges in identifying the shortest path.

3.2 Incorporating Known Relative Ordering

One notable feature of DirectLiNGAM is its capability to incorporate prior knowledge to enhance overall results by allowing users to specify which directed edges are required, forbidden, or unknown [31]. In this study, we introduce an enhancement to LiNGAM-SPP to allow for integrating prior knowledge. Unlike DirectLiNGAM, where the exact edges need to be specified, our implementation only requires specifying the relative order. In practical terms, this means we can assert that one feature causes another while still allowing for the possibility of having intermediary features, or mediators, between them.

To implement this, we modify the shortest path algorithm to selectively skip nodes that violate the specified order. The path formulation of LiNGAM-SPP naturally lends itself to this task. Each node in the graph (e.g., Figure 1) contains information about relative ordering, indicating which features have been selected and which are yet to be explored. Specifically, if a feature is absent from the subscripts, it is positioned earlier in the causal order. For instance, referencing the same graph (Figure 1), if we assert that x_1 precedes x_2 , then nodes with subscript 1 but not 2—such as $\{r_3^{(2)}, r_1^{(2)}\}$ and $\{r_1^{(2,3)}\}$ —should be skipped. This is because they imply that x_2 comes before x_1 , which violates the known ordering.

3.3 Predicting Causal Graph Properties from Path Distributions

The utility of the path formulation extends beyond finding the shortest path. We discovered that path enumeration, representing the distribution of total path lengths of all possible orderings, reveals crucial insights into graph properties. Specifically, we observed and will demonstrate that

the path distribution can be used to infer graph properties such as the presence of unmeasured confounders (an essential assumption to verify, especially for LiNGAM), the sparsity of the graph, and, to some extent, the reliability of PLR DirectLiNGAM and PLR LiNGAM-SPP.

We have observed, and will show in the results section, that clear patterns emerge in the path distributions in different cases, i.e. whether or not there are unmeasured confounders and differing graph sparsity. To take advantage of this insight – that the path distribution informs us about graph properties – we extract standardized moments to capture the shape of the distribution. Specifically, we compute the standardized moments of the log-transformed path lengths. These standardized moments will then serve as features in models trained to predict the various graph properties. The standardized moment is defined as follows:

$$\tilde{\mu}_k = \frac{E[(X - \mu)^k]}{(\text{Var}[X - \mu])^{k/2}} \quad (11)$$

Here, $\tilde{\mu}_k$ denotes the k -th standardized moment, and X represents the log-transformed path lengths.

After extracting the standardized moments, we train the following models using various popular machine learning algorithms (k NN [24], Random Forest [24], XGBoost [3], CatBoost [5], and AdaBoost [24]):

- (1) **Confounder Detector** - a classifier to detect the presence of unmeasured confounders
- (2) **Sparsity Estimator** - a classifier and a regression model to estimate graph sparsity
- (3) **DirectLiNGAM and LiNGAM-SPP Performance Predictors** - classifier and regression models to predict the reliability of these methods

Although enumerating all possible paths can be done through brute force, we opted for a more efficient approach using Zero-Suppressed Binary Decision Diagrams (ZDDs). ZDDs are compact data structures that efficiently represent a family (or set) of sparse subsets from a finite ordered universe U [19, 37]. In the context of graph theory, the diagram may also represent a family of subgraphs $G' \subseteq G$ for a graph $G = (V, E)$. The frontier-based search algorithm provides a way to construct the diagram representing subgraphs, particularly paths, in a graph by setting the universe as the set of edges $U = E$ [15].

While the TdZdd library is commonly used for ZDD construction and set operations, its C++ implementation posed compatibility issues with our Python pipeline. Hence, we adopted the graphillion library instead, which offers a Python interface for ZDD operations. Although the standardized moments were calculated post hoc in our implementation, direct computation using ZDD operations, as demonstrated by [17], is also possible.

4 RESULTS

4.1 Improving LiNGAM-SPP with PLR

As previously discussed, we propose using PLRs as the mutual information estimator for LiNGAM-SPP, which we refer to as PLR LiNGAM-SPP. To evaluate the performance of PLR LiNGAM-SPP, we conducted experiments on a data generating process adapted from the DirectLiNGAM paper [31], with modifications to incorporate simulated unmeasured confounders. This data generating process differs from, but is more comprehensive than, the one utilized in the original LiNGAM-SPP studies [34, 35], so the results here may be different from these studies. Furthermore, we assessed the method's efficacy in practical settings by testing it on real-world datasets, comparing the results with those obtained from DirectLiNGAM. This validation demonstrates the method's utility beyond simulated scenarios.

4.1.1 Data Generating Process. Our data generating process was adapted from [31], which we extended to incorporate cases with unmeasured confounders, following the framework outlined in [9, 36], where LiNGAM with unmeasured confounders can be represented as:

$$\mathbf{x} = \mathbf{B}\mathbf{x} + \mathbf{\Lambda}\mathbf{f} + \mathbf{e} \quad (12)$$

In this equation, \mathbf{x} represents the observed data, \mathbf{B} is a $p \times p$ matrix where p is the number of features, \mathbf{f} is the latent confounder vector, and \mathbf{e} is the non-Gaussian noise. The matrix $\mathbf{\Lambda}$, with elements λ_{ij} , denotes the connection strength between f_j and x_i . Additionally, each unmeasured confounder should have at least 2 children, and the matrix $\mathbf{\Lambda}$ should be of full column rank [9, 36]. To implement this, we performed the following steps:

- (1) We initialized the matrix \mathbf{B} by creating a $p \times p$ lower triangular matrix with elements randomly drawn from a uniform distribution in the interval $[-1.5, -0.5] \cup [0.5, 1.5]$, following [31, 32].
- (2) To introduce sparsity into the graph, we applied an element-wise product with a Bernoulli distribution matrix, following the approach of [14, 31]. The success probability parameter of this Bernoulli distribution determines the sparsity of the graph.
- (3) For modeling non-Gaussian noise and confounders, we used the set of 18 non-Gaussian distributions used in [1, 31]. Each noise term and confounder were randomly sampled from this set. Moreover, we scaled these distributions to ensure their variances fell within the interval $[1, 3]$, as in [31, 32]. In addition, we included a scaling parameter for the confounders called "confounding strength".
- (4) To construct $\mathbf{\Lambda}$, we generated its columns sequentially. For each column to be added, we first selected two variables to be influenced. Subsequently, we created a binary column vector by sampling it from a Bernoulli distribution, where the probability of success, an adjustable parameter, may be interpreted as the "confoundedness" of the graph. The two selected variables and the binary vector are combined to create a vector determining which features are to be confounded. In effect, each column of $\mathbf{\Lambda}$ will have at least 2 nonzero elements, even if "confoundedness" is set to 0. Finally, before appending the column to $\mathbf{\Lambda}$, we make sure that it is not equal to any of the existing columns, ensuring that $\mathbf{\Lambda}$ remains full rank.

In summary, our data generating process is designed to capture a broad range of linear non-Gaussian processes. It allows us to control various parameters such as the number of features p , sample size N , sparsity, confoundedness, confounding strength, and the number of confounders. In the following sections where we present results of simulations, the simulations used sparsity drawn from a uniform distribution $U(0, 1)$, confounding strength 10^s with s drawn from $U(1, 2)$, the number of confounders (if present) is randomly selected from $\{1, 2, 3\}$, and confoundedness is drawn from $U(0, 1)$.

4.1.2 Comparing PLR LiNGAM-SPP with Existing Methods. To showcase the effectiveness of this enhancement, we compare our proposed method, PLR LiNGAM-SPP, with other existing methods: PLR DirectLiNGAM [12], k NN LiNGAM-SPP [34], and copent (copula entropy) LiNGAM-SPP [35]. Following the methodology in the original k NN LiNGAM-SPP paper [34], we used the following definition for the k NN-based mutual information estimator [16]:

$$I(X, Y) = \psi(k) - \langle \psi(n_x + 1) + \psi(n_y + 1) \rangle + \psi(N) \quad (13)$$

where $\psi(\cdot)$ represents the digamma function. To implement this, we adapted code from the feature selection module of the `sklearn` [24] library, extending it to accommodate a one-to-many variable setting, i.e. $I((X_1, X_2, \dots, X_{m-1}), X_m)$, by redefining n_x in Eq. 13 to represent the number of points in the $(m - 1)$ -dimensional space, as outlined by [16]. Meanwhile, we use the Python package `copent` [18] for computing the copula entropy in `copent LiNGAM-SPP`. Finally, performance was

Table 1. Comparison of Average Ordering Errors (E_o) Across Various Methods and Scenarios

		Without Confounders				With Confounders			
	Sample Size (N)	100	250	500	1000	100	250	500	1000
p	Method								
5	PWLR LiNGAM-SPP	0.29	0.28	0.23	0.21	0.46	0.45	0.42	0.39
	PWLR DirectLiNGAM	0.29	0.28	0.23	0.22	0.46	0.45	0.42	0.40
	Copent LiNGAM-SPP	0.40	0.41	0.38	0.39	0.43	0.40	0.43	0.42
	kNN LiNGAM-SPP	0.29	0.23	0.22	0.18	0.40	0.37	0.35	0.33
10	PWLR LiNGAM-SPP	0.33	0.24	0.21	0.18	0.44	0.40	0.37	0.34
	PWLR DirectLiNGAM	0.32	0.25	0.22	0.19	0.44	0.41	0.37	0.36
	Copent LiNGAM-SPP	0.49	0.48	0.50	0.49	0.46	0.46	0.45	0.46
	kNN LiNGAM-SPP	0.48	0.40	0.35	0.30	0.49	0.43	0.39	0.35
15	PWLR LiNGAM-SPP	0.33	0.24	0.19	0.16	0.41	0.36	0.35	0.29
	PWLR DirectLiNGAM	0.32	0.25	0.21	0.18	0.42	0.37	0.33	0.32
	Copent LiNGAM-SPP	0.51	0.50	0.51	0.52	0.48	0.48	0.49	0.49
	kNN LiNGAM-SPP	0.56	0.51	0.45	0.38	0.54	0.49	0.46	0.40

evaluated using the same error metric as previous LiNGAM-SPP papers [34, 35], where the ordering error, denoted as E_o , is defined by:

$$E_o = \frac{2r}{p(p-1)}, \quad (14)$$

where p represents the number of features, and r is the count of pairs in the wrong order. This essentially counts the fraction pairs in the incorrect order.

As previously mentioned, both k NN and copent LiNGAM-SPP require the tuning of the k parameter, which is not possible in practical settings. However, for the purpose of comparison, instead of parameter tuning, we set k to 5%, 10%, and the square root of the sample size (N), then selected the best-performing configuration. Table 1 presents results for various scenarios. The reported values represent the average ordering errors, E_o , across 250 trials for each scenario. The results and conclusions drawn from this comparison may differ from the previous LiNGAM-SPP studies, since a different, albeit more general, data generating process was used for the simulations.

While k NN LiNGAM-SPP excels for $p = 5$, PLR LiNGAM-SPP outperforms in most cases for larger p , with DirectLiNGAM closely trailing. A paired t-test reveals that, overall, PLR LiNGAM-SPP shows a statistically significant improvement over DirectLiNGAM with a p-value of 5.22×10^{-5} .

Interestingly, the performance disparity between PLR LiNGAM-SPP and DirectLiNGAM widens as the number of features (p) increases. We hypothesize that LiNGAM-SPP demonstrates greater robustness, particularly with longer sequences, owing to its ability for backtracking and correction. In contrast to DirectLiNGAM, which is prone to error propagation—wherein a mistake in one step compromises subsequent steps—LiNGAM-SPP, utilizing Dijkstra’s algorithm, exhibits a mechanism for error correction: If an incorrect feature is selected in one step, subsequent steps are more likely to yield large mutual information values. In such instances, Dijkstra’s algorithm can backtrack to explore alternative paths with smaller overall values.

Furthermore, Table 2 presents the average run times for the same cases. As expected, DirectLiNGAM, being a greedy algorithm, exhibits the fastest runtimes. Meanwhile, the runtimes of copent and k NN LiNGAM-SPP, both of which rely on the k NN mutual information estimator, tend to increase with sample size (N). Despite this trend, copent LiNGAM-SPP has the smallest runtimes

Table 2. Average Runtime Comparison Across Various Methods and Scenarios (Note: m represents minutes)

		Without Confounders				With Confounders			
p	Sample Size (N)	100	250	500	1000	100	250	500	1000
	MI Estimator								
5	PWLR LiNGAM-SPP	0.44s	0.44s	0.45s	0.46s	0.43s	0.45s	0.44s	0.46s
	PWLR DirectLiNGAM	0.04s	0.04s	0.04s	0.05s	0.04s	0.04s	0.04s	0.05s
	Copent LiNGAM-SPP	0.06s	0.11s	0.3s	1.1s	0.07s	0.13s	0.35s	1.3s
	kNN LiNGAM-SPP	0.27s	0.39s	0.72s	1.8s	0.26s	0.37s	0.65s	1.7s
10	PWLR LiNGAM-SPP	6.8s	6.9s	6.9s	6.1s	6.4s	7.2s	7s	7.6s
	PWLR DirectLiNGAM	0.26s	0.27s	0.3s	0.36s	0.26s	0.27s	0.31s	0.36s
	Copent LiNGAM-SPP	0.4s	0.6s	1.3s	4.6s	0.48s	0.7s	1.6s	5.5s
	kNN LiNGAM-SPP	32s	45s	1.4m	3.5m	32s	44s	1.3m	3.4m
15	PWLR LiNGAM-SPP	2.2m	1.6m	1.2m	1.5m	1.4m	3.6m	2.8m	3.2m
	PWLR DirectLiNGAM	0.83s	0.9s	0.98s	1.2s	0.84s	0.92s	1s	1.2s
	Copent LiNGAM-SPP	1.3s	1.8s	3.4s	11s	1.6s	2.1s	4.3s	14s
	kNN LiNGAM-SPP	37m	48m	84m	206m	36m	49m	85m	205m

Table 3. Performance Comparison of PLR DirectLiNGAM and PLR LiNGAM-SPP on Real-World Datasets

		Known Edges		DirectLiNGAM		LiNGAM-MMI	
Dataset	p	Req.	Forb.	Req.	Forb.	Req.	Forb.
sachs [27]	11	20	0	10	0	10	0
yacht-hydrodynamics [6]	7	1	15	0	2	0	2
abalone [20]	8	0	17	0	4	0	4
airfoil-self-noise [2]	6	0	11	0	6	0	6
wine-quality-red [4]	12	2	11	1	7	2	2
wine-quality-white [4]	12	2	11	2	4	2	1

out of all LiNGAM-SPP methods. On the other hand, k NN LiNGAM-SPP runs notably slower; for instance, at $p = 15$, the runtime can extend to hours. However, while copent LiNGAM-SPP is faster, its performance remains subpar. Overall, PLR LiNGAM-SPP presents the most favorable compromise between runtime efficiency and performance, with the added advantage of not requiring parameter tuning.

4.1.3 Testing on Real-world Data. To evaluate PLR LiNGAM-SPP on real-world data, we sourced datasets from the CMU-Clear (Carnegie Mellon University Causal Learning and Reasoning Group) list of benchmarks, accessible on GitHub: <https://github.com/cmu-phil/example-causal-datasets>. Our criteria for selection included datasets with continuous features and known ground truth. Additionally, we restricted our choices to datasets with $p \leq 20$ due to the computational demands of the LiNGAM-SPP method for larger values of p .

To derive the causal graph from LiNGAM-SPP, we adapted code from the `lingam` package [13]. Specifically, after getting the causal order, we used the same sparse regression as DirectLiNGAM to identify which edges are zero [31, 39]. Table 3 provides the ground truth for each dataset, indicating required and forbidden edges, along with the edges captured by PLR DirectLiNGAM and PLR LiNGAM-SPP. The ground truth originally included tiers, which we converted into forbidden edges,

Table 4. Computed Edges with Prior Knowledge

Prior Knowledge p	Without Confounders				With Confounders			
	0%	25%	50%	75%	0%	25%	50%	75%
4	9	9	8	6	9	9	8	6
8	35	34	27	18	39	40	37	22
12	107	99	81	42	184	198	174	74

given that later tiers cannot cause earlier ones. For more details about the datasets and the provided ground truth, please refer to the GitHub repository.

The results in Table 3 reveal that for the wine-quality (red and white) datasets, PLR LiNGAM-SPP outperforms PLR DirectLiNGAM, capturing fewer forbidden edges and more required edges. For the other datasets, both methods yield identical results. This observation aligns with the findings in Table 1, indicating that PLR LiNGAM-SPP is more robust for longer sequences. Moreover, this suggests that, in most cases, PLR LiNGAM-SPP performs at least as well as PLR DirectLiNGAM.

4.2 Incorporating Known Relative Ordering

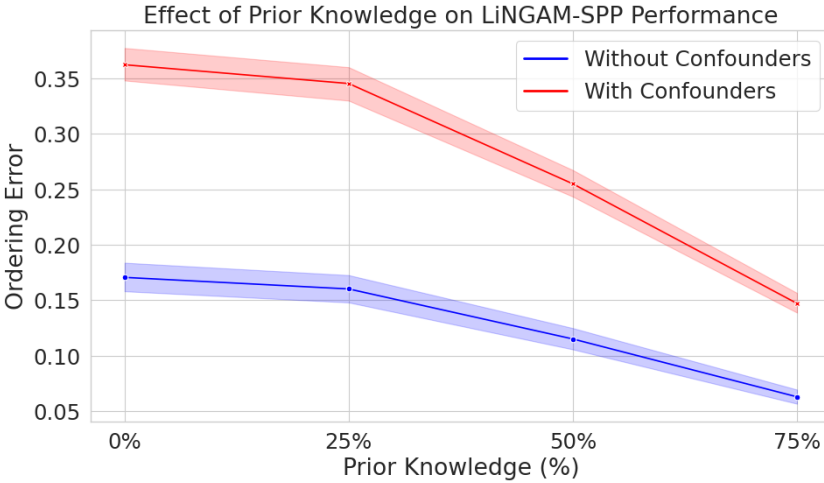


Fig. 2. Performance Impact of Prior Knowledge: Combined results for $p = 4, 8, 12$.

We demonstrate the impact of incorporating prior knowledge on performance in Figure 2 and Table 4. To quantify the extent of prior knowledge, we express it as a percentage of variables with specified orderings. For example, if $p = 8$, 50% knowledge means that the relative ordering of 4 variables is given. In this demonstration, the input is the relative ordering of 2 or more variables, which we then convert to variable pairs, e.g., (1, 2, 3) implies (1, 2), (2, 3), (1, 3). However, it is also possible to manually specify pairs. As expected, incorporating more prior knowledge improves performance (Figure 2) and generally reduces the traversed number of edges (Table 4).

Relative ordering provides a more flexible way of incorporating prior knowledge, which is valuable because we do not always know the exact edges. It is more common for us to know the

relative ordering rather than the exact edges. For instance, in most applications, it is known that nothing can affect a person’s age, sex, and other background variables, so these must be positioned earlier in the ordering relative to other variables. Another example is incorporating temporal information, where features with time-related attributes may exist, and we only know the temporal order but not necessarily the ordering among the features within the same time slice.

4.3 Predicting Causal Graph Properties from Path Distributions

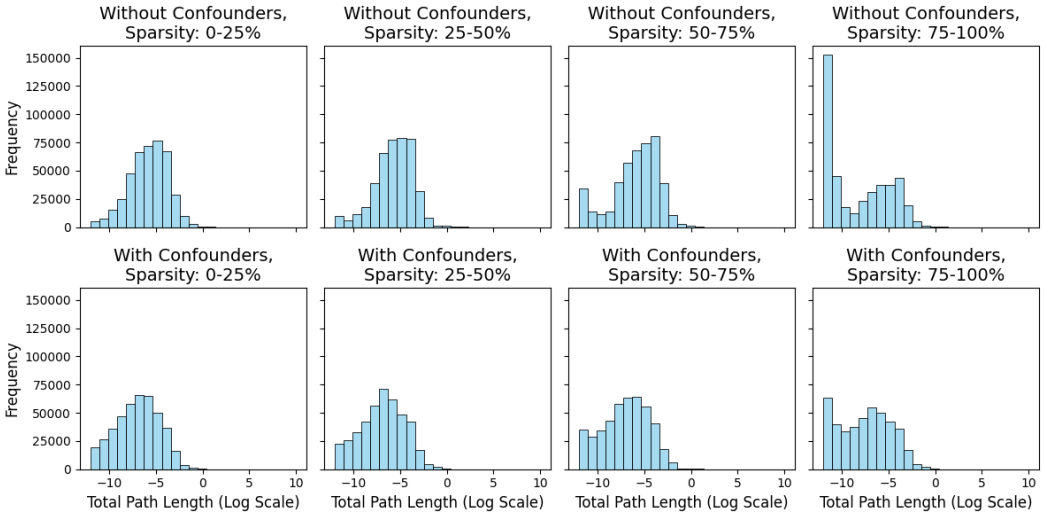


Fig. 3. Log-transformed Path Distributions for Various Scenarios

Our motivation for predicting causal graph properties from path distributions is drawn from the observations depicted in Figure 3. These histograms show the combined log-transformed PLR path distributions for $p = 4, 5, 6$ (where p represents the number of features), using the same data generating process and simulation configurations as detailed in preceding sections. Notably, discernible patterns emerge in the path distributions across different scenarios: More complex scenarios, characterized by the presence of confounders or higher graph sparsity, exhibit an increased frequency of shorter paths. This observation suggests that determining the correct order becomes more challenging and ambiguous under such conditions.

4.3.1 Confounder Detector. Detecting unmeasured confounders is crucial, especially for LiNGAM, which assume the absence of unmeasured confounders. In this section, we developed a confounder detector—a classifier for detecting the presence of unmeasured confounders. The features used were the 3rd to the 30th standard moments of the log-transformed path distribution, and the target is binary: 1 if there are confounders and 0 if none. We then trained different classifier models, as shown in Table 5. Note that, for demonstration purposes, these models were not fine-tuned, so there is still room for improving these results. Regardless, the models demonstrate good performance, with CatBoost achieving the highest AUC of 0.78, indicating good discrimination between the classes.

Figure 4 shows the ROC curve and the confusion matrix from CatBoost evaluated on the test set. The optimal threshold is determined using Youden’s J statistic, which selects the threshold that maximizes the difference between the true positive and false positive rates. This threshold can be

Table 5. Comparison of Confounder Detectors Trained with Various Classifiers

Model	AUC	Precision	Recall	Accuracy	Optimal Threshold
<i>k</i> NN	0.6537	0.5918	0.7365	0.6142	0.4000
Random Forest	0.7608	0.6883	0.7465	0.7042	0.3300
XGBoost	0.7665	0.6955	0.7400	0.7080	0.3278
CatBoost	0.7829	0.6957	0.7740	0.7178	0.3271
AdaBoost	0.6997	0.6557	0.7540	0.6790	0.4972

changed depending on the precision and sensitivity requirements of the use case. However, for the optimal threshold, we see that the CatBoost model exhibited good sensitivity (77.4% recall) and precision (69.6%).

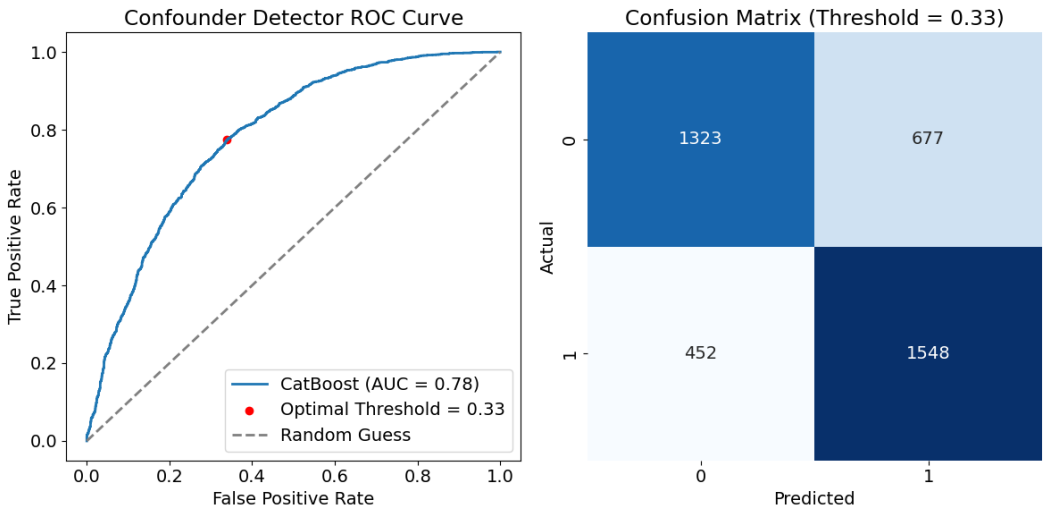


Fig. 4. ROC Curve and Confusion Matrix of the Confounder Detector (CatBoost)

Thus, we have demonstrated that it is possible to detect unmeasured confounders with reasonable performance using information from the shape of the path distribution captured through the standardized moments.

4.3.2 Sparsity Estimator. Another task we explore is predicting graph sparsity using standard moments. Using the same features as the confounder detector, we initially create a classifier predicting whether sparsity is greater than 0.5. Table 6 presents the results from different models. Similar to the confounder detector, CatBoost achieved the highest AUC of 0.77. While CatBoost’s precision and recall are remarkable, AdaBoost offers slightly better precision, and XGBoost provides slightly better recall—choosing between them depends on the specific use case. Figure 5 displays the ROC curve and confusion matrix for CatBoost. Once again, it demonstrates good AUC, precision, and recall, indicating the model’s effective discrimination.

In addition to the classifier, we explored creating a regression model using the same features, with the target being the actual sparsity (ranging from 0 to 1). Table 7 compares results from different models. Among them, AdaBoost delivered the best coefficient of determination R^2 of 0.16,

Table 6. Comparison of Sparsity Estimators Trained with Various Classifiers

Model	AUC	Precision	Recall	Accuracy	Optimal Threshold
<i>k</i> NN	0.6262	0.5949	0.6054	0.5905	0.4000
Random Forest	0.7286	0.7174	0.5640	0.6660	0.3400
XGBoost	0.7551	0.6773	0.7443	0.6902	0.2161
CatBoost	0.7744	0.7043	0.7217	0.7050	0.2647
AdaBoost	0.7579	0.7285	0.6438	0.6975	0.4958

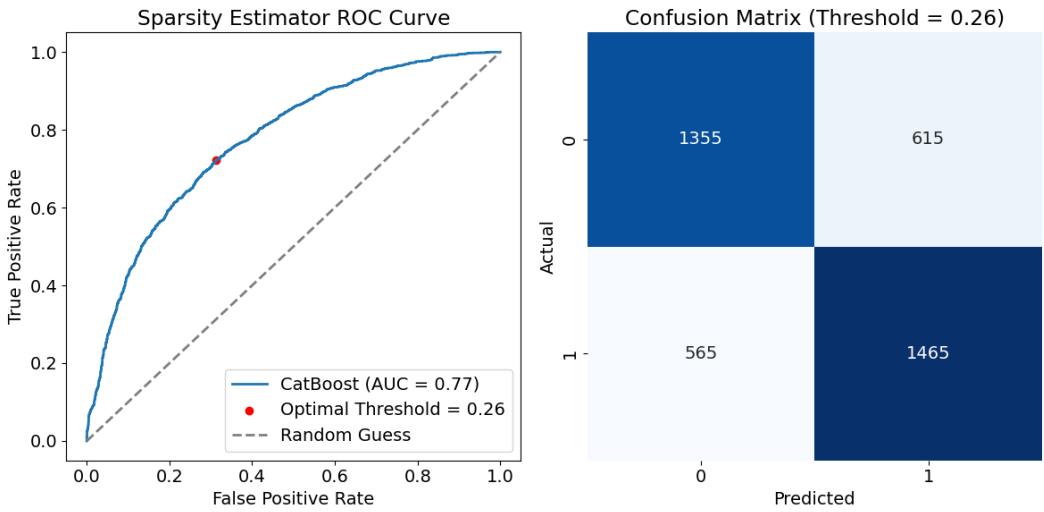


Fig. 5. ROC Curve and Confusion Matrix of the Sparsity Estimator (CatBoost)

Table 7. Regression Results for Graph Sparsity Prediction

Model	R^2	RMSE	MAE
<i>k</i> NN	-0.0804	0.3002	0.2460
Random Forest	0.0824	0.2766	0.2240
XGBoost	0.0645	0.2793	0.2269
CatBoost	0.1027	0.2736	0.2229
AdaBoost	0.1568	0.2652	0.2252

indicating that the shape of the distribution (i.e., the standard moments) can explain some of the variance in sparsity. AdaBoost also yields an RMSE of 0.27, reasonably estimating sparsity.

4.3.3 Performance Predictors. Thus far, we have created models for detecting confounders and graph sparsity. These two properties are crucial for evaluating the performance of DirectLiNGAM and LiNGAM-SPP, as cases involving confounders or sparse graphs tend to pose greater challenges and lead to poorer performance for these methods. However, we wanted to test if it were possible to directly predict the performance of these methods, so we developed classifiers for PLR DirectLiNGAM and PLR LiNGAM-SPP to predict whether they would produce the correct causal

Table 8. Comparison of Performance Predictors Trained with Various Classifiers

Model	LiNGAM-SPP				DirectLiNGAM			
	AUC	Precision	Recall	Accuracy	AUC	Precision	Recall	Accuracy
<i>k</i> NN	0.641	0.155	0.613	0.617	0.638	0.147	0.594	0.615
Random Forest	0.822	0.272	0.752	0.768	0.821	0.239	0.801	0.725
XGBoost	0.799	0.237	0.774	0.721	0.800	0.311	0.648	0.821
CatBoost	0.822	0.333	0.698	0.826	0.821	0.306	0.711	0.809
AdaBoost	0.790	0.292	0.672	0.799	0.789	0.269	0.711	0.777

Table 9. Regression Results for Performance Prediction

Model	LiNGAM-SPP			DirectLiNGAM		
	R^2	RMSE	MAE	R^2	RMSE	MAE
<i>k</i> NN	-0.1012	0.2150	0.1674	-0.0853	0.2149	0.1672
Random Forest	0.0836	0.1961	0.1472	0.0853	0.1973	0.1487
XGBoost	0.0388	0.2008	0.1499	0.0319	0.2030	0.1521
CatBoost	0.1162	0.1926	0.1441	0.1009	0.1956	0.1465
AdaBoost	0.2109	0.1820	0.1436	0.2096	0.1834	0.1449

ordering. In other words, the target is 1 if the predicted causal order is entirely correct. Table 8 showcases the results. For the LiNGAM-SPP performance predictor, CatBoost delivered the best AUC of 0.82. However, given the relatively small number of instances with exact correct ordering (as it is more likely to get some of the ordering wrong than to get everything right), while sensitivity (recall) is reasonable at 0.70, precision is not very high (0.33), indicating a significant number of false positives.

Meanwhile, for the DirectLiNGAM performance predictor, both Random Forest and CatBoost provided similar AUCs of 0.82, with Random Forest having the best recall at 0.80, while another model, XGBoost, exhibited the highest precision at 0.31. Similar to the LiNGAM-SPP case, sensitivity of the models is good, but precision is not as high, suggesting a notable presence of false positives. We also explored fitting regression models to the ordering score of LiNGAM-SPP and DirectLiNGAM, with the results shown in Table 9. For the LiNGAM-SPP case, AdaBoost emerged as the best model, achieving the highest R^2 of 0.21, indicating its ability to explain some variance in the ordering score. AdaBoost also boasted the lowest RMSE of 0.18, reasonably pinpointing the ordering score within a reasonable range. Similarly, for DirectLiNGAM, AdaBoost also outperformed other models, achieving an R^2 of 0.21 and an RMSE of 0.18.

4.3.4 Path Sampling. One drawback of path enumeration is the factorial increase of the number of edges with the number of features. To address the impracticality of using the entire path distribution (especially in cases with large p), we opt for a more practical solution—sampling from the path distribution to compute the standardized moments. As mentioned earlier, ZDDs provide this functionality by sampling from the subset of graphs it represents. Here, we demonstrate the tradeoff between path sample size and model performance (AUC), revealing that sufficiently good performance for the models discussed earlier can still be achieved without resorting to the entire path distribution. Table 10 presents the performance of the models under various path sampling sizes. In this demonstration, we limit the training and testing to $p = 7$ since $7! = 5040$,

Table 10. Model Performance Under Different Path Sampling Sizes

Path Sample Size	Confounder Detector	Sparseness Estimator	Performance Predictors	
			LiNGAM-SPP	DirectLiNGAM
100	0.7453	0.7317	0.6811	0.6880
250	0.7498	0.7553	0.7436	0.7241
500	0.7824	0.7734	0.7772	0.7792
1000	0.7979	0.7856	0.7980	0.7969
2500	0.8183	0.7932	0.8140	0.8075
All Paths (5040)	0.8204	0.7939	0.8480	0.8538

which is sufficiently large for our evaluation. The table illustrates that the models' AUC generally increases with the path sample size, approaching the performance of the full path distribution. For instance, even at a path sample size of 2500, the confounder detector and sparsity estimator already achieved AUCs that are sufficiently close to those obtained using the full path distribution. While the performance predictors for the same path sample size still have a slightly larger gap, the performance is already acceptable. This demonstrates the trade-off between path sample size and model performance. For larger values of p , even a fraction of the possible paths may already yield satisfactory performance.

5 CONCLUSION

In this study, we addressed a critical limitation of LiNGAM-SPP by eliminating the need for parameter tuning. Our modification, using the PLR [12] in place of the k NN-based mutual information estimators from earlier LiNGAM-SPP studies [34, 35], not only eliminated the need for fine-tuning but also demonstrated superior performance and computational efficiency on simulated data. Furthermore, the modified LiNGAM-SPP we propose, PLR LiNGAM-SPP, proves to be more stable than DirectLiNGAM, significantly outperforming it specially in simulations with more features. Our method performs at least as well as DirectLiNGAM on real-world data and, in some cases, outperforms it by capturing more required edges and fewer forbidden edges.

Additionally, we introduced a functionality to LiNGAM-SPP for incorporating prior knowledge. Notably, our approach allows for specifying relative orderings rather than exact edges, offering increased flexibility. The integration of prior knowledge improved the method's performance and reduced the number of edges traversed.

Furthermore, we extended the LiNGAM-SPP method by leveraging the entire path distribution. Specifically, the standardized moments of the path distribution were used as features to create models that estimate certain properties of the causal graph. We created a confounder detector, a sparsity estimator, and predictors for DirectLiNGAM and PLR LiNGAM-SPP performance. The confounder detector and sparsity estimator showed robust performance, achieving high AUCs of 0.783 and 0.774 respectively. Meanwhile, although the DirectLiNGAM and LiNGAM-SPP performance predictors achieved AUCs of 0.822 and 0.821 respectively, they exhibited a higher rate of false positives due to the inherent challenge in getting the exact causal ordering.

We also acknowledge the limitations of our study, such as the intractability of path enumeration for large p , which led us to limit our demonstration to a small number of features. This limitation is somewhat addressed using the sampling feature of ZDDs, but constructing the ZDD itself becomes more difficult (requiring more memory) as p increases.

In conclusion, our study proposed an enhancement to the current LiNGAM-SPP and demonstrated other ways to leverage the path search formulation of the causal ordering problem. While further research is needed to address limitations and provide theoretical grounding, our results offer a promising direction for inferring properties of the causal graph from observational data.

REFERENCES

- [1] Francis R. Bach and Michael I. Jordan. 2003. Kernel Independent Component Analysis. *J. Mach. Learn. Res.* 3, null (mar 2003), 1–48. <https://doi.org/10.1162/153244303768966085>
- [2] Thomas Brooks, D. Pope, and Michael Marcolini. 2014. Airfoil Self-Noise. UCI Machine Learning Repository. DOI: <https://doi.org/10.24432/C5VW2C>.
- [3] Tianqi Chen and Carlos Guestrin. 2016. XGBoost: A Scalable Tree Boosting System. In *Proceedings of the 22nd ACM SIGKDD International Conference on Knowledge Discovery and Data Mining*. 785–794. <https://doi.org/10.1145/2939672.2939785> arXiv:1603.02754 [cs].
- [4] Paulo Cortez, A. Cerdeira, F. Almeida, T. Matos, and J. Reis. 2009. Wine Quality. UCI Machine Learning Repository. DOI: <https://doi.org/10.24432/C56S3T>.
- [5] Anna Veronika Dorogush, Vasily Ershov, and Andrey Gulin. 2018. CatBoost: gradient boosting with categorical features support. arXiv:1810.11363 [cs.LG]
- [6] J. Gerritsma, R. Onnink, and A. Versluis. 2013. Yacht Hydrodynamics. UCI Machine Learning Repository. DOI: <https://doi.org/10.24432/C5XG7R>.
- [7] Clark Glymour, Kun Zhang, and Peter Spirtes. 2019. Review of Causal Discovery Methods Based on Graphical Models. *Frontiers in Genetics* 10 (2019). <https://www.frontiersin.org/articles/10.3389/fgene.2019.00524>
- [8] Arthur Gretton, Kenji Fukumizu, Choon Teo, Le Song, Bernhard Schölkopf, and Alex Smola. 2007. A Kernel Statistical Test of Independence. In *Advances in Neural Information Processing Systems*, J. Platt, D. Koller, Y. Singer, and S. Roweis (Eds.), Vol. 20. Curran Associates, Inc. https://proceedings.neurips.cc/paper_files/paper/2007/file/d5cfead94f5350c12c322b5b664544c1-Paper.pdf
- [9] Patrik Hoyer, Dominik Janzing, Joris M Mooij, Jonas Peters, and Bernhard Schölkopf. 2008. Nonlinear causal discovery with additive noise models. In *Advances in Neural Information Processing Systems*, Vol. 21. Curran Associates, Inc. <https://proceedings.neurips.cc/paper/2008/hash/f7664060cc52bc6f3d620bcedc94a4b6-Abstract.html>
- [10] Aapo Hyvärinen. 1997. New Approximations of Differential Entropy for Independent Component Analysis and Projection Pursuit. In *Advances in Neural Information Processing Systems*, M. Jordan, M. Kearns, and S. Solla (Eds.), Vol. 10. MIT Press. https://proceedings.neurips.cc/paper_files/paper/1997/file/6d9c547cf146054a5a720606a7694467-Paper.pdf
- [11] A. Hyvärinen. 1998. *New Approximations of Differential Entropy for Independent Component Analysis and Projection Pursuit*. WorkingPaper. MIT Press. 273–279 pages.
- [12] Aapo Hyvärinen and Stephen M. Smith. 2013. Pairwise Likelihood Ratios for Estimation of Non-Gaussian Structural Equation Models. *Journal of Machine Learning Research* 14, 4 (2013), 111–152. <http://jmlr.org/papers/v14/hyvarinen13a.html>
- [13] Takashi Ikeuchi, Mayumi Ide, Yan Zeng, Takashi Nicholas Maeda, and Shohei Shimizu. 2023. Python package for causal discovery based on LiNGAM. *Journal of Machine Learning Research* 24, 14 (2023), 1–8. <http://jmlr.org/papers/v24/21-0321.html>
- [14] Markus Kalisch and Peter Bühlmann. 2007. Estimating High-Dimensional Directed Acyclic Graphs with the PC-Algorithm. *Journal of Machine Learning Research* 8, 22 (2007), 613–636. <http://jmlr.org/papers/v8/kalisch07a.html>
- [15] Jun Kawahara, Takeru Inoue, Hiroaki Iwashita, and Shin ichi Minato. 2017. Frontier-based Search for Enumerating All Constrained Subgraphs with Compressed Representation. *IEICE Transactions on Fundamentals of Electronics, Communications, and Computer Sciences Vol. E100-A No. 9 (2017)*, 1773–1784.
- [16] Alexander Kraskov, Harald Stögbauer, and Peter Grassberger. 2004. Estimating mutual information. *Phys. Rev. E* 69, 6 (June 2004), 066138. <https://doi.org/10.1103/PhysRevE.69.066138> Publisher: American Physical Society.
- [17] Brian Godwin Lim, Renzo Roel Tan, Jun Kawahara, Shin ichi Minato, and Kazushi Ikeda. Submitted. A Recursive Framework for Evaluating Moments Using Zero-Suppressed Binary Decision Diagrams. *IEEE Access* (Submitted).
- [18] Jian Ma and Zengqi Sun. 2011. Mutual information is copula entropy. *Tsinghua Science and Technology* 16, 1 (2011), 51–54. [https://doi.org/10.1016/S1007-0214\(11\)70008-6](https://doi.org/10.1016/S1007-0214(11)70008-6)
- [19] Shinichi Minato. 1993. Zero-Suppressed BDDs for Set Manipulation in Combinatorial Problems. *Proceedings of the 30th International Design Automation Conference (1993)*, 272–277.
- [20] Warwick Nash, Tracy Sellers, Simon Talbot, Andrew Cawthorn, and Wes Ford. 1995. Abalone. UCI Machine Learning Repository. DOI: <https://doi.org/10.24432/C55C7W>.
- [21] Judea Pearl. 2000. *Causality: models, reasoning, and inference*. Cambridge University Press, Cambridge, U.K. ; New York.

- [22] Judea Pearl, Madelyn Glymour, and Nicholas P. Jewell. 2016. *Causal inference in statistics: a primer*. Wiley, Chichester, West Sussex.
- [23] Judea Pearl and Dana Mackenzie. 2018. *The book of why: the new science of cause and effect*. Basic Books, New York.
- [24] Fabian Pedregosa, Gaël Varoquaux, Alexandre Gramfort, Vincent Michel, Bertrand Thirion, Olivier Grisel, Mathieu Blondel, Peter Prettenhofer, Ron Weiss, Vincent Dubourg, et al. 2011. Scikit-learn: Machine Learning in Python. *Journal of Machine Learning Research* 12 (2011), 2825–2830.
- [25] Jonas Peters, Dominik Janzing, and Bernhard Schölkopf. 2017. *Elements of causal inference: foundations and learning algorithms*. The MIT Press, Cambridge, Massachusetts.
- [26] Donald B Rubin. 2005. Causal Inference Using Potential Outcomes: Design, Modeling, Decisions. *J. Amer. Statist. Assoc.* 100, 469 (March 2005), 322–331. <https://doi.org/10.1198/016214504000001880>
- [27] Karen Sachs, Omar Perez, Dana Pe'er, Douglas A. Lauffenburger, and Garry P. Nolan. 2005. Causal Protein-Signaling Networks Derived from Multiparameter Single-Cell Data. *Science* 308, 5721 (2005), 523–529. <https://doi.org/10.1126/science.1105809> arXiv:<https://www.science.org/doi/pdf/10.1126/science.1105809>
- [28] Bernhard Schölkopf, Francesco Locatello, Stefan Bauer, Nan Rosemary Ke, Nal Kalchbrenner, Anirudh Goyal, and Yoshua Bengio. 2021. Toward Causal Representation Learning. *Proc. IEEE* 109, 5 (May 2021), 612–634. <https://doi.org/10.1109/JPROC.2021.3058954>
- [29] Shohei Shimizu. 2014. Lingam: Non-Gaussian Methods for Estimating Causal Structures. *Behaviormetrika* 41, 1 (Jan. 2014), 65–98. <https://doi.org/10.2333/bhmk.41.65>
- [30] Shohei Shimizu, Patrik O Hoyer, Aapo Hyvarinen, and Antti Kerminen. 2006. A Linear Non-Gaussian Acyclic Model for Causal Discovery. (2006), 28.
- [31] Shohei Shimizu, Takanori Inazumi, Yasuhiro Sogawa, Aapo Hyvarinen, Yoshinobu Kawahara, Takashi Washio, Patrik O Hoyer, and Kenneth Bollen. 2011. DirectLiNGAM: A Direct Method for Learning a Linear Non-Gaussian Structural Equation Model. (2011), 24.
- [32] Ricardo Silva, Richard Scheine, Clark Glymour, and Peter Spirtes. 2006. Learning the Structure of Linear Latent Variable Models. *Journal of Machine Learning Research* 7, 8 (2006), 191–246. <http://jmlr.org/papers/v7/silva06a.html>
- [33] Peter Spirtes and Kun Zhang. 2016. Causal discovery and inference: concepts and recent methodological advances. *Applied Informatics* 3, 1 (Feb. 2016), 3. <https://doi.org/10.1186/s40535-016-0018-x>
- [34] Joe Suzuki and Tianle Yang. 2022. An Generalized LiNGAM when confounder is present. (2022).
- [35] Joe Suzuki and Tian-Le Yang. 2024. Generalization of LiNGAM that allows confounding. arXiv:2401.16661 [cs.LG]
- [36] Tatsuya Tashiro, Shohei Shimizu, Aapo Hyvarinen, and Takashi Washio. 2013. ParceLiNGAM: A causal ordering method robust against latent confounders. arXiv:1303.7410 [stat.ML]
- [37] Takahisa Toda, Toshiki Saitoh, Hiroaki Iwashita, Jun Kawahara, and Shin ichi Minato. 2017. ZDDs and Enumeration Problems: State-of-the-Art Techniques and Programming Tool. *Computer Software Vol. 34 No. 3* (2017), 97–120.
- [38] Liuyi Yao, Zhixuan Chu, Sheng Li, Yaliang Li, Jing Gao, and Aidong Zhang. 2021. A Survey on Causal Inference. *ACM Trans. Knowl. Discov. Data* 15, 5, Article 74 (may 2021), 46 pages. <https://doi.org/10.1145/3444944>
- [39] Hui Zou. 2006. The Adaptive Lasso and Its Oracle Properties. *J. Amer. Statist. Assoc.* 101, 476 (2006), 1418–1429. <https://doi.org/10.1198/016214506000000735> arXiv:<https://doi.org/10.1198/016214506000000735>

Received xx Month 20xx; revised xx Month 20xx; accepted xx Month 20xx